Chapter 6

Control of solid-state transformer-enabled DC microgrids

Xu She[1], Alex Huang[2], Xunwei Yu[3], and Yizhe Xu[4]

Source: DC Distribution Systems and Microgrids,2018
Publication date October 2018

6.1 Introduction

With the world-wide energy shortage and deterioration of existing power grid, microgrid becomes one of the hottest research directions in the power engineering area. Considering DC nature of many key components in the smart grid, such as photovoltaic (PV), battery, fuel cell, super capacitor, etc., as well as many DC type loads, such as light-emitting diode, DC microgrid has received more attention recently since it brings the opportunity for boosting the efficiency by eliminating the unnecessary power conversion stages. However, the existing DC microgrid can only interface with the distribution system by using a heavy and bulky passive line frequency transformer plus a rectifier, which has large space and heavy weight. Developing a more compact and active grid interface to enable an intelligent DC microgrid system is still a research focus. In this chapter, the solid-state transformer (SST)-enabled DC microgrid is presented. In addition, two system control strategies, namely, the centralized power management and hierarchical power management strategies, are proposed. In addition, an improved control strategy is proposed for increasing the penetration of distributed renewable energy resources (DRER) integration, which controls SST-enabled DC microgrid as a solid-state synchronous machine (SSSM). With the proposed control concept, frequency and voltage stability are improved in case of high-power intermittence at either DC load or DRER side. Design examples are given to illustrate the main characteristics of the presented system and control schemes.

6.2 Solid-state transformer-based microgrid: architecture and benefits

The SST is a power electronic device that replaces the traditional 50/60 Hz power transformer by means of high-frequency transformer isolated AC–AC conversion

[1]Electric Power, GE Global Research, United States
[2]Electric and Computer Engineering, University of Texas Austin, United States
[3]Intersil Corporation, United States
[4]Grid Bridge Inc., United States

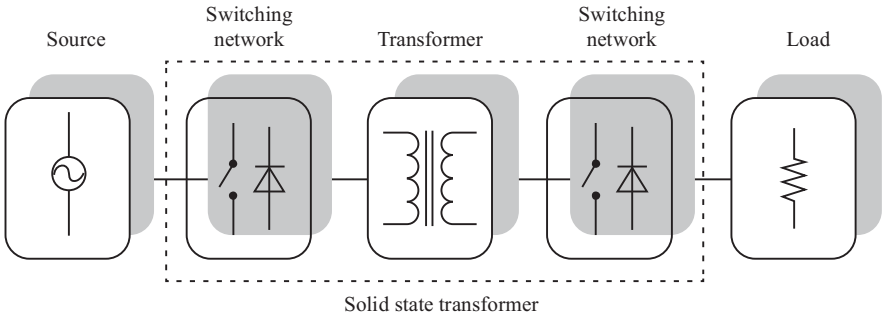

Figure 6.1 Configuration of solid-state transformer (SST) from source to load

technique, which is represented in Figure 6.1 [1]. The basic operation of the SST is firstly to convert the 50/60 Hz AC voltage to a high-frequency one (normally in the range of several to tens of kilohertz), then this high-frequency voltage is stepped up/down by a high-frequency transformer with significantly decreased volume and weight, and finally shaped back into the desired 50/60 Hz voltage to feed the load. Therefore, the first advantage that the SST can offer is its reduced volume and weight compared with traditional transformers. It is further seen from the configuration of the SST that some other potential functionalities that are not owned by the traditional transformers may be obtained. First, the use of solid-state semiconductor devices and circuits makes the voltage and current regulation a possibility. This brings promising features such as power flow control, voltage sag compensation, fault current limitation, and others, which are not possible for traditional transformers. Second, voltage source converters connected from the secondary terminal of the SST could readily support a regulated DC bus, which could be connected to DC microgrid, enabling this new microgrid architecture.

Figure 6.2 demonstrates the proposed SST-based DC microgrid system [2]. The AC loads are connected to the AC mains of SST, and the DC sources and loads are connected to the DC mains for minimizing the conversion stages. The high-voltage side of the SST is connected to the distribution system; thus, the conventional transformer is eliminated. The presence of SST can also isolate the distribution system from the residential side; therefore, the fault on one side will not affect another. Furthermore, the high-voltage AC/DC converter in the distribution system side can realize power factor regulation, enabling the Var compensation capability. Therefore, the SST-based microgrid is more compact and shows superior characteristics over conventional AC and DC microgrids.

Similar like the traditional microgrids, different power management strategies could be applied. In the following sections, both the centralized and hierarchical power management strategies are presented. In addition, SSSM control concepts are also proposed to enhance the system stability at high-power intermittence condition. Design examples are given to demonstrate the feasibility of the proposed SST-enabled DC microgrid.

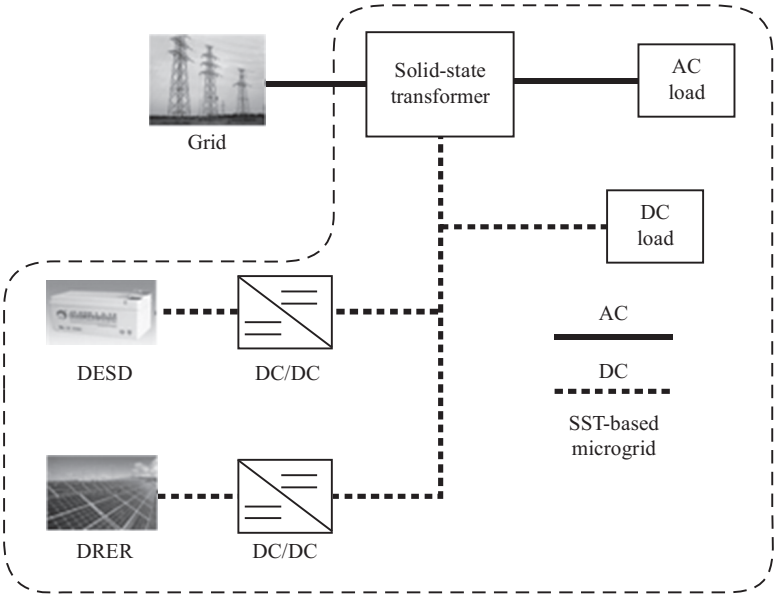

Figure 6.2 SST-based microgrid architecture: DESD and DRER. DESD, distributed energy storage device; DRER, distributed renewable energy resource

6.3 Centralized power management of solid-state transformer-based DC microgrid

6.3.1 Power management strategy

In the centralized power management strategy, an intelligent energy management (IEM) algorithm should be developed. The operating modes of DC microgrid can be defined as shown in Figure 6.3, where three modes are identified, namely, active grid interaction mode, passive grid interaction mode, and islanding mode.

In the passive grid interaction mode, SST controls the DC voltage. Although the DC microgrid is interfaced with the distribution system, it balances the power within the network without any power being exchanged with SST. In the active grid interaction mode, due to the limited power balancing capability of the DC microgrid under certain operating conditions, additional power is transferred between SST and DC microgrid. In the islanding mode, SST stops working and the battery regulates the DC bus. The DC microgrid supplies the additional power for the load at AC side whenever extra power is available. The assumption is made in this chapter that the SST, as the backup of DC microgrid, can always supply enough power under the grid interaction mode by an optimized design. The whole power management algorithm aims at maximizing the utilization of PV and battery and minimizing the burden of existing AC grid, as well as ensuring a high reliability of the power system.

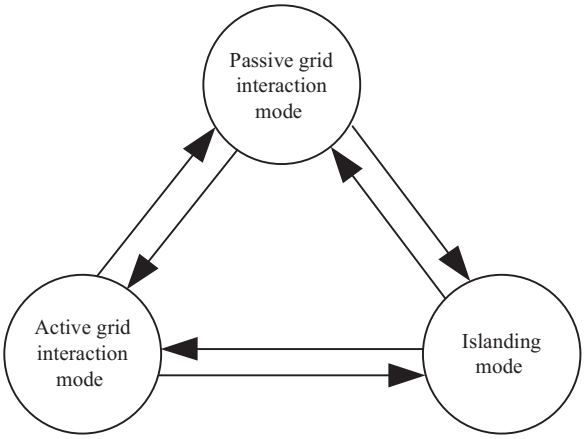

Figure 6.3 Operating modes and transitions of SST-enabled microgrid

If divided in detail, there are ten possible operating modes for the presented system, and they are shown in Figure 6.4. The nomenclature in the flowchart is defined in Table 6.1.

The division of the modes mainly depends on the operating status of the distribution system, battery state of charge (SOC), and battery power. These modes are summarized and explained as below.

Mode 1: PV operates in maximum power point tracking (MPPT) mode, battery stops working, and SST supplies the additional power for DC load.

Mode 2: PV operates in MPPT mode, battery operates in discharging power limitation mode, and SST supplies the additional power for DC load.

Mode 3: PV operates in MPPT mode, battery balances the power within DC microgrid, and SST only supplies power for AC load.

Mode 4: PV operates in MPPT mode, battery operates in charging power limitation mode, and SST absorbs the additional power from DC microgrid.

Mode 5: PV operates in MPPT mode, battery stops working, and SST absorbs the additional power from DC microgrid.

Mode 6: Part of loads is shed and the system operates in either Mode 8 or Mode 9, depending on the operating condition.

Mode 7: Part of loads is shed and the system operates in Mode 8, Mode 9, or Mode 10, depending on the operating condition.

Mode 8: PV operates in MPPT mode and battery operates in voltage tracking mode.

Mode 9: PV operates in power tracking mode for supplying the total load power. In this mode, the power reference of PV converter is set to

$$P_{pv} = P_{load\_DC} + P_{load\_DC} + P_{b\,\max} \tag{6.1}$$

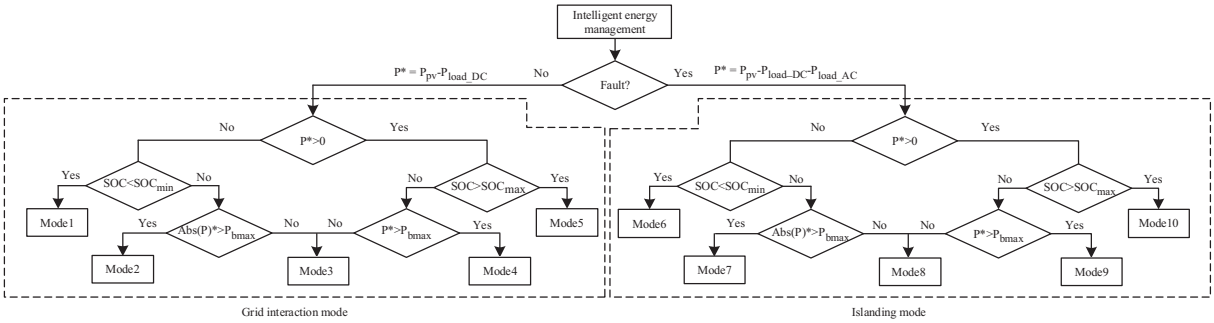

Figure 6.4 Intelligent energy management system diagram of SST using PV and battery

Table 6.1 Nomenclature for IEM system

P_{pv}	Power of PV
P_{load_DC}	Power of DC load
P_{load_AC}	Power of AC load
SOC_{min}	Minimum allowed SOC
SOC_{max}	Maximum allowed SOC
P_{bmax}	Maximum allowed battery power

The battery operates in voltage tracking mode, and its absorbed power is fixed to charging power limitation automatically.

Mode 10: PV operates in power tracking mode for supplying the total load power and the battery controls the DC bus voltage while no power is delivered to the load.

As it can be seen above, Modes 1–5 belong to the active grid interaction mode. Mode 3 belongs to the passive grid interaction mode. Modes 6–10 belong to the islanding mode. In the presented power management strategy, the matched battery capacity needs to be designed, and the system should operate in Mode 3 for most of the time. Only when the local power balancing capability is limited, a transition to other modes occurs. Thus, the presented IEM system can maximize the utilization of PV and battery and minimize the effect to the existing AC power grid architecture.

6.3.2 Case study

To verify the presented intelligent power management algorithm, a simulation platform is established by using the average modeling technique. The average model instead of the switching model is preferred for this large power system since it speeds up the simulation without losing the capability of capturing the main characteristics of the system. In the developed simulation platform, the power rating of SST is set to 20 kVA, the maximum power of PV under the irradiation of 1 kW/m^2 is set to 8 kW, and the maximum charging/discharging power of the battery pack is set to 6 kW. Different load profiles are adopted to test different cases. Only parts of the cases are tested for demonstrating the main characteristics of the system due to page limitations.

6.3.2.1 Passive grid interaction (Mode 3)

To emulate the operating Mode 3, which is the passive grid interaction mode, the AC load for SST is set to 10 kW, and DC load is set to 4 kW. The key operating waveforms are shown in Figure 6.5.

The irradiation of PV is gradually changing from 300 W/m^2 to 1 kW/m^2, and then back to 300 W/m^2 to emulate the irradiation of a day, as shown in Figure 6.5(a). Figure 6.5(b) shows the power distribution of the presented system.

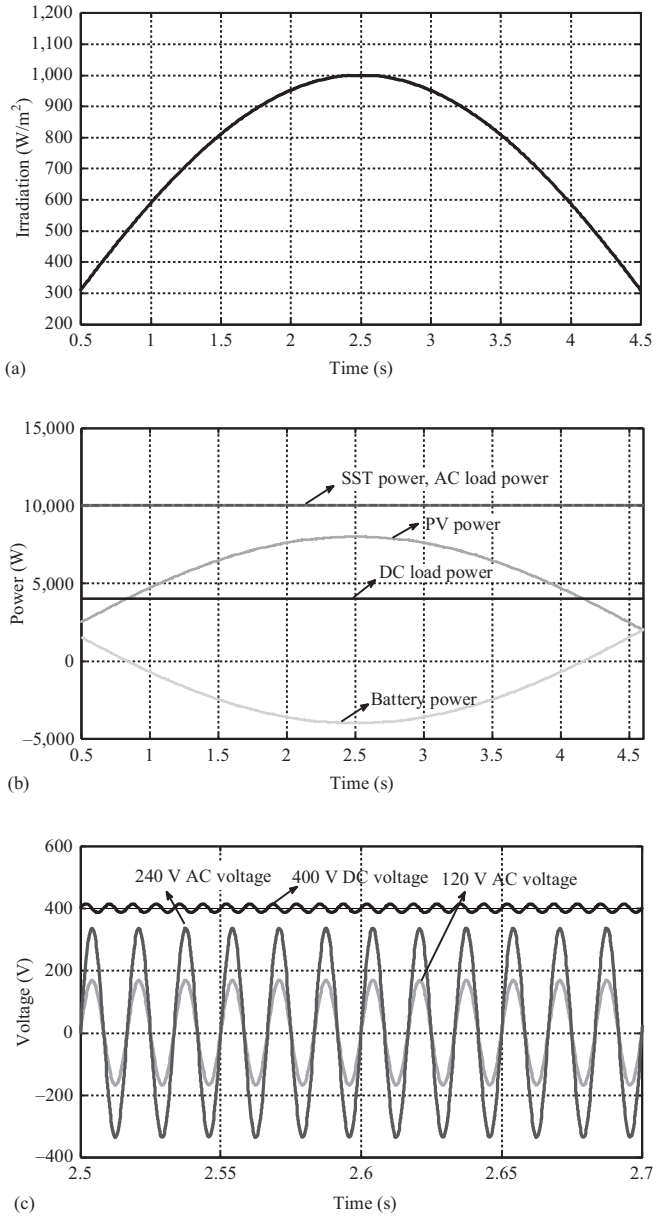

Figure 6.5 Key operating waveforms in Mode 3 of the system in Figure 6.2: (a) irradiation of PV panel, (b) power distribution of the system, (c) low-voltage terminal waveforms, (d) high-voltage terminal waveforms, (e) SOC of the battery

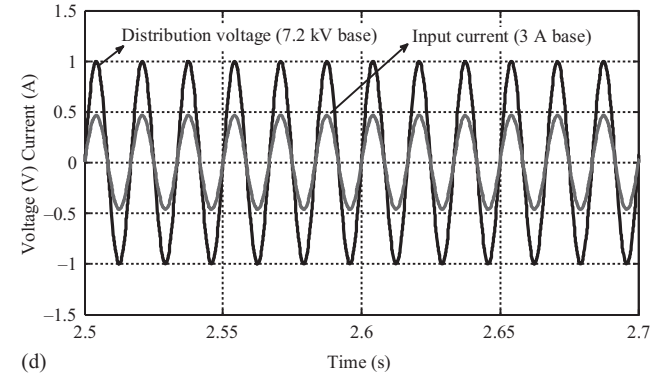

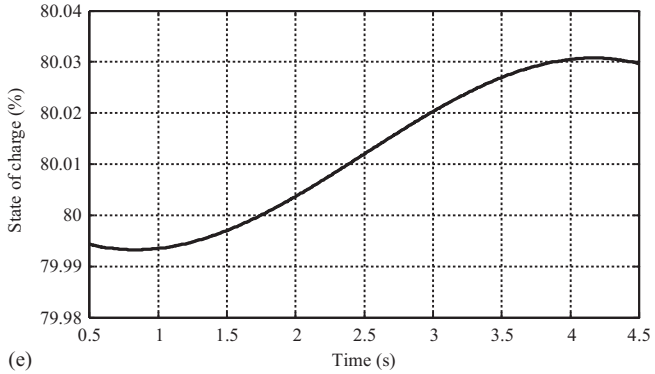

Figure 6.5 (*Continued*)

The power of the PV has the same trend with the irradiation. SST only supplies the AC load power, which is 10 kW. Since the power of the battery is within its limitation, it can balance the power between DC load and PV. Figure 6.5(c) shows the regulated low-voltage terminal waveforms, including 400 V DC and 120/240 V AC. In Figure 6.5(d), the SST input voltage and current are depicted. The current is in phase with voltage, indicating a unity power factor operation. The battery SOC is described by Figure 6.5(e), where the initial SOC is set to 80%. The trend of SOC depends on the direction of current. A positive battery current discharges the battery and a negative battery current charges the battery in the presented system in Figure 6.2.

6.3.2.2 Transition from passive grid interaction mode to active grid interaction mode (Mode 2 to Mode 3)

The transition from passive grid interaction mode to active grid interaction mode is demonstrated. Mode 2 and Mode 3 are chosen to verify the operation, in which the AC load is set to 10 kW and the DC load is set to 1 kW. Key operating waveforms

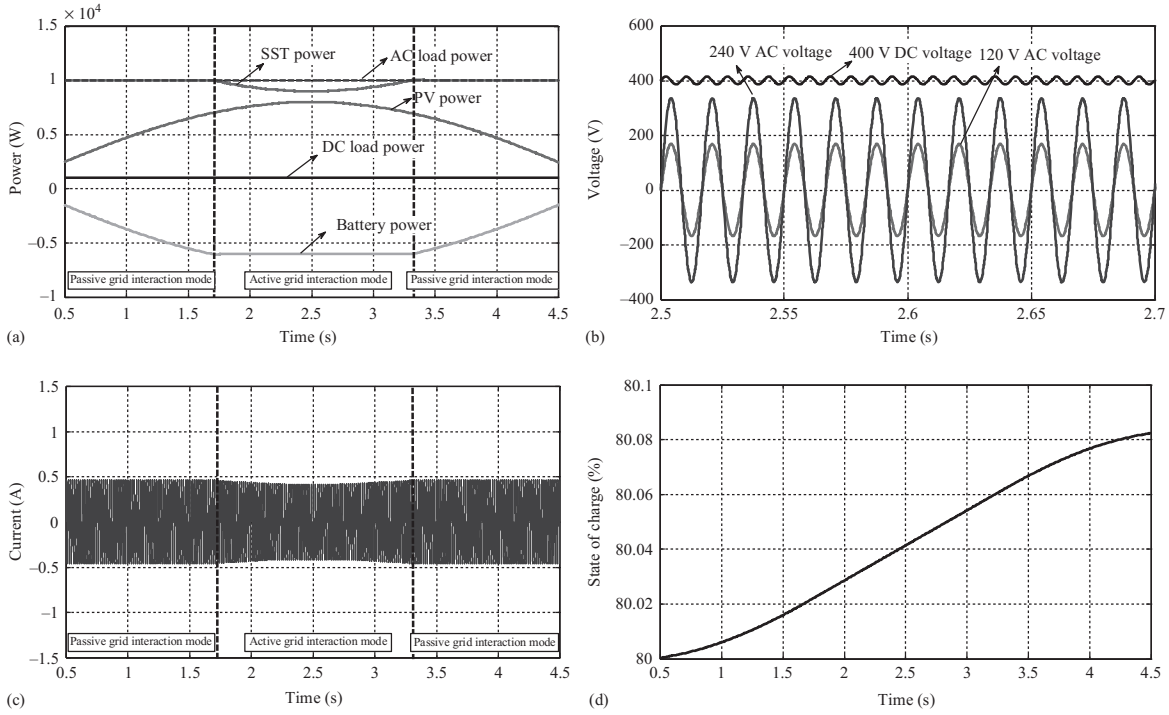

Figure 6.6 Key operating waveforms during mode transition (Mode 2 to Mode 3): (a) power distribution of the system, (b) low-voltage terminal waveforms, (c) high-voltage terminal current (3 A base), (d) SOC of the battery pack

are shown in Figure 6.6. Figure 6.6(a) shows the power distribution of the system. At the beginning, the power of battery pack is within the limitation and the system operates in the passive grid interaction mode (Mode 3). With the irradiation of PV panel increasing, the charging power of the battery also increases. Then the system transits into the active grid interaction mode (Mode 2) when battery power reaches the 6 kW limitation. The additional power of DC microgrid flows into the SST and supplies to the AC load. After that, the PV power decreases to a certain value and the system operates back to passive grid interaction mode. Figure 6.6(b) depicts the well-regulated AC and DC voltages. Figure 6.6(c) demonstrates the input current of SST, which shows the same trend with the SST power since the input voltage is fixed. Figure 6.6(d) shows the SOC of the battery and it increases continuously. As it can be seen, the transition between these two modes is smooth and occurs automatically.

6.3.2.3 Islanding mode (Mode 8)

The microgrid transits into the islanding mode when fault occurs in the distribution system. How to detect the grid fault is not addressed here. For the demonstration purpose, operation of Mode 8 is chosen and the waveforms are shown in Figure 6.7, where the AC load is set to 4.5 kW and the DC load is set to 1 kW.

Power distribution of the system is shown in Figure 6.7(a), where the battery balances the power between PV and load (both AC and DC load). Figure 6.7(b) shows the key waveforms at the low-voltage terminal. It can be seen that the DC bus voltage is regulated well by the battery converter. Figure 6.7(c) shows the SOC of the battery pack. When the battery current is positive, the SOC decreases. Otherwise, the SOC increases.

6.3.2.4 Islanding mode transition (Mode 8 to Mode 9)

Finally, the mode transition in the islanding mode is studied. In the study, the AC load is set to 1 kW, and the DC load changes from 2 to 0 kW at 2.7 s. The key operating waveforms are shown in Figure 6.8. Figure 6.8(a) shows the power distribution in this case. Before the DC load changes, the system operates in mode 8 and the battery can balance the power between the PV and the load. Thus, the PV operates in MPPT mode for extracting the maximum power available. When the DC load is cut at 2.7 s, the power command of the battery is larger than 6 kW and battery then operates in charging power limitation mode. The PV no longer operates in MPPT mode and transits to power tracking mode. Figure 6.8(b) illustrates the 400-V DC voltage during the mode transition. Due to the cutting down of the DC load, a voltage overshoot occurs and recovers within 0.05 s. The SOC of the battery is given in Figure 6.8(c), and the battery is charged continuously. Clearly, the transition between different islanding modes is smooth.

6.3.3 Summary

A centralized power management strategy is presented for SST-enabled microgrid system with PV and battery. It renders the coordinate management of power

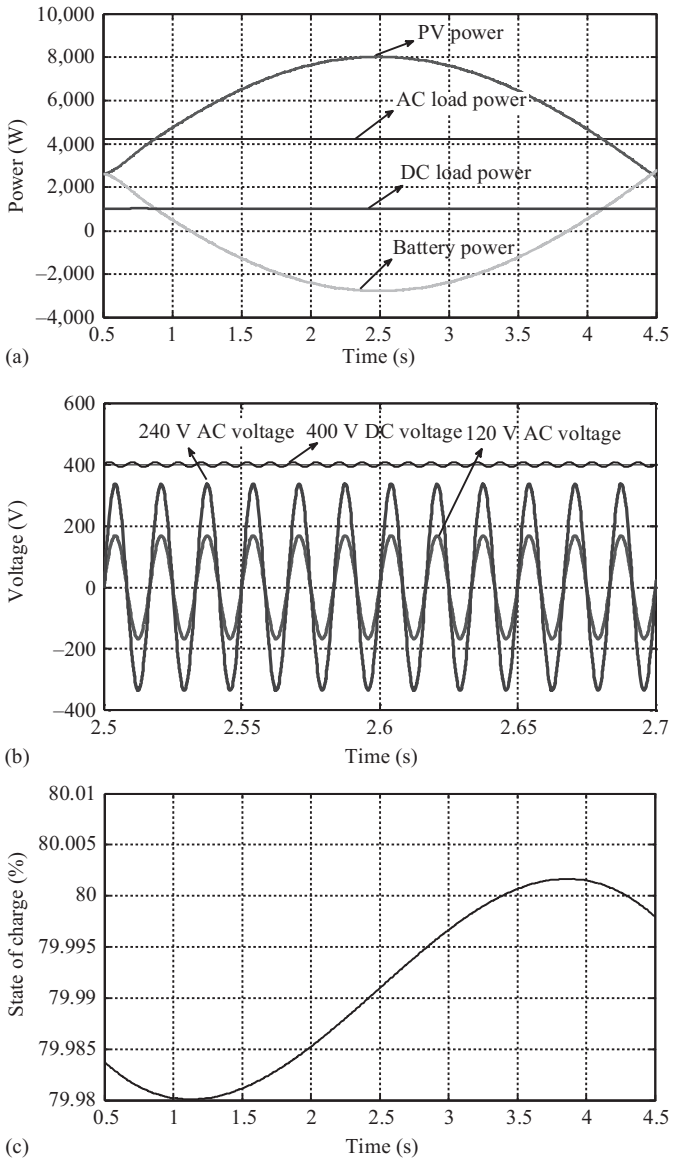

Figure 6.7 Mode 8 key operating waveforms: (a) power distribution of the system, (b) low-voltage terminal waveforms, (c) SOC of battery pack

between DC microgrid and distribution system. In addition, the impact of the established DC microgrid to the existing power grid can be minimized, which promises a better reliability and stability. The presented strategy is verified through some simulation studies.

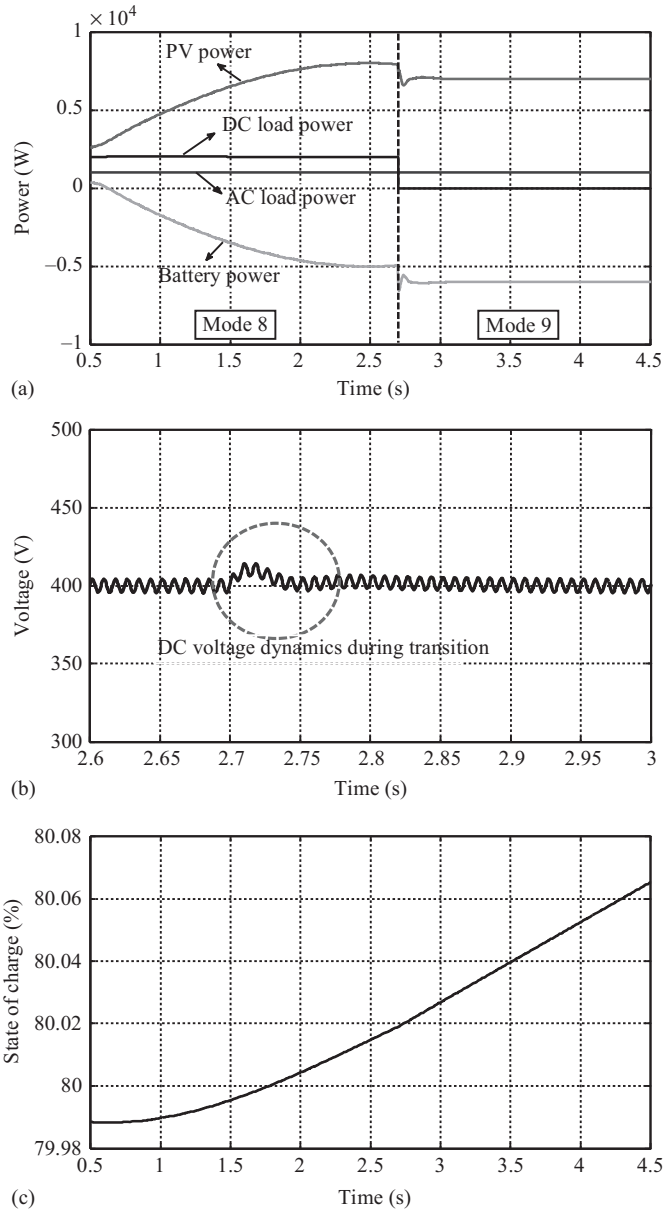

Figure 6.8 Key operating waveforms during mode transition (Mode 8 and Mode 9): (a) power distribution of the system, (b) 400-V DC bus voltage dynamics, (c) SOC of battery pack

6.4 Hierarchical power management of solid-state transformer-enabled DC microgrid

6.4.1 Power management strategy

The hierarchical control is a hybrid method, which combines the advantages of both centralized and distributed control and can be served as standard method for the microgrid [3]. As shown in Figure 6.9, the system control strategy frame is categorized into three layers: primary control, secondary control, and tertiary control. The primary control is the distributed control, which ensures that the microgrid system can operate without communication. Therefore, the primary control usually takes effect at the micro-second level, which is basically the same level as the converter control. All the local information, including the voltage, current, SOC, etc., are sent to the upper controller, which implements the tertiary control and secondary control through a bidirectional communication link. Here, the DC microgrid is enabled by the SST, and therefore, the SST controller is used as the upper controller [4]. The objective of the secondary control is to recover the microgrid bus voltage to achieve seamless transfer as the system switches from islanding mode to SST-enabled mode. The time scale of the secondary control is on the order of milliseconds to seconds.

6.4.1.1 Primary control algorithm

When the system operates in islanding mode, the battery needs to regulate the DC bus voltage alone. Therefore, (6.2) can be obtained.

$$C_{eq}V_{DC}\frac{dV_{DC}}{dt} = (P_{DC\_Load} - P_{Battery} - P_{PV}) \tag{6.2}$$

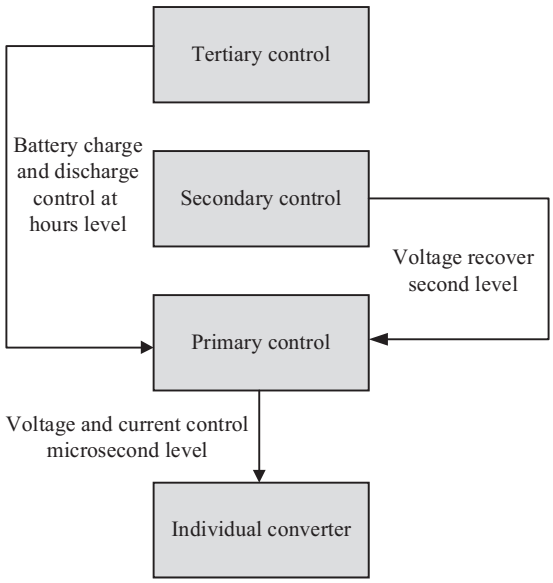

Figure 6.9 Hierarchical control frame

Since P_{PV} is equal or larger than zero, the power direction of battery is determined by the difference between the P_{PV} and P_{DC_Load}. For example, the power of the battery will be larger than zero when P_{DC_Load} is larger than P_{PV}, while the power of the battery will be less than zero when P_{DC_Load} is smaller than P_{PV}.

Basically, the primary control algorithm is based on DC bus signal control, and therefore, the distributed control can be achieved. In this control algorithm, the DC bus voltage is no longer a fixed value, but varies in a certain range in the islanding mode.

The DC bus voltage range is defined as from 360 to 400 V in the presented system design. In islanding mode, only the battery is used to regulate the DC bus voltage. Droop control is adopted for battery control with the expression shown in (6.3):

$$V_b = V_0 - R_b I_b \tag{6.3}$$

where V_b is the reference for the DC bus voltage, V_o is bus voltage value without load and it is set to 380 V, R_b is the virtual output impedance, and I_b is battery output current. For the PV module, it always operates in MPPT mode to deliver power to the system. Noted here, the load management is involved in the primary control. The load is divided into the critical load and the noncritical load. When the PV has no output power to the system, the bus voltage will drop. The battery has to source more power to the load and the battery SOC will decrease rapidly. To ensure that the DC microgrid can operate as long as possible in islanding mode, the battery SOC has to be considered. Therefore, to avoid battery SOC dropping fast, the noncritical load will be shed from the system when the bus voltage decreases below some preset threshold (370 V). When the bus voltage recovers to a certain value, 380 V for instance, the noncritical load can be reconnected to the system. The primary control diagram is shown in Figure 6.10.

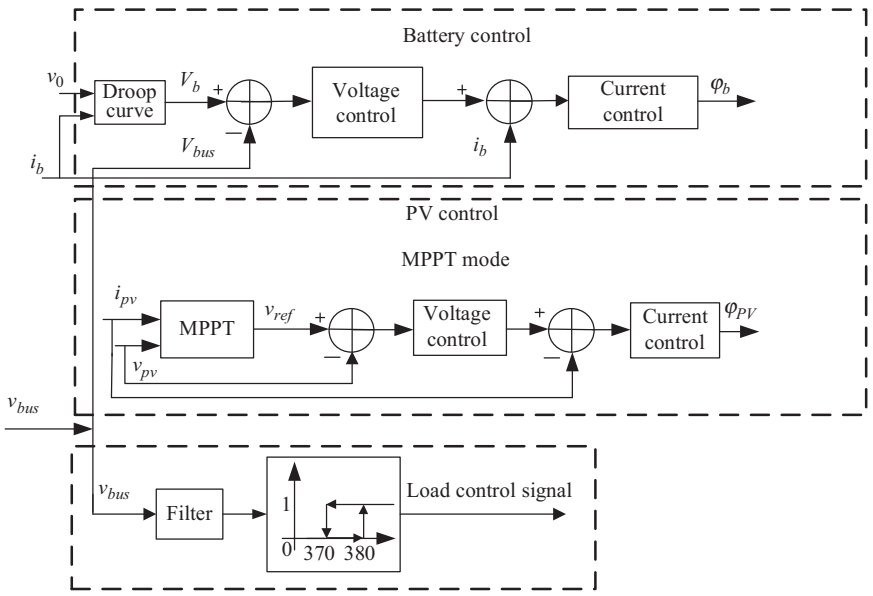

Figure 6.10 Primary control diagram of the DC microgrid system

6.4.1.2 Secondary control algorithm

Since the DC bus voltage is regulated by droop control in islanding mode, the bus voltage might deviate from the SST DC terminal output voltage. To achieve the seamless transfer from islanding mode to SST-enabled mode, the secondary control is adopted. Specifically, when the DC microgrid needs to connect to the SST, the secondary control-enabled signal is triggered. The SST DC terminal voltage is sensed and compared with the DC microgrid bus voltage. Then the voltage difference is processed by a compensator and the output is sent to the battery unit via the low-bandwidth communication to restore the DC microgrid bus voltage (see Figure 6.11). Since the PV and load control do not contribute to regulating the DC bus voltage, their control remains unchanged as shown in Figure 6.10. Due to the space limitations, only the battery module control is depicted in Figure 6.11.

The controller can be represented as

$$V_s = k_{sp}(V_{SST\_dcout} - V_{bus}) + (k_{si}(V_{SST\_dcout} - V_{bus})/s) \tag{6.4}$$

where k_{sp} and k_{si} are the control parameters for the secondary control. Therefore, the droop control of the battery becomes

$$V_b = V_0 - R_b I_b + V_s \tag{6.5}$$

Based on (6.5), the key function of the secondary control is to shift the droop curve (see Figure 6.12). When the SST's DC output voltage is higher than DC microgrid

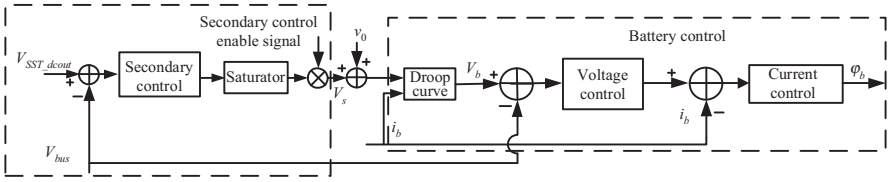

Figure 6.11 Secondary control diagram of the DC microgrid system

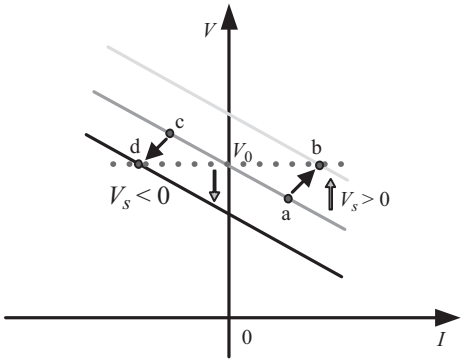

Figure 6.12 Droop curve shift with secondary control

bus voltage, V_s is larger than zero and the droop curve is shifted upward (battery operation point from a to b), and vice versa (battery operation point from c to d).

It is noticed that since the low bandwidth communication is adopted, the secondary controller's time step should agree with that of the communication to prevent secondary controller saturation.

6.4.1.3 Tertiary control algorithm

An appropriate SOC value is necessary for the battery to supply the DC bus voltage while operating in islanding mode. Therefore, SOC is included in the tertiary control. When the system operates in SST-enabled mode, the DC bus voltage will be regulated by the SST, and therefore, SST DC output is a stiff bus as seen from the DC microgrid. Then the battery charge or discharge can be determined by the SST DC voltage and battery droop curve. There are two options for managing the battery SOC in SST-enabled mode. The first is to change the SST DC terminal output voltage, and the second is to shift the battery droop curve, both of which are detailed below.

Change SST DC terminal output voltage

Since the PV and load control do not contribute to regulate the DC bus voltage, their control is the same as shown in Figure 6.10. Only the battery module control is depicted in Figure 6.13. As shown in Figure 6.13, the SOC is evaluated and processed by the current reference selection block. If the SOC reaches the H_{SOC} (upper limit for SOC) or L_{SOC} (lower limit for SOC), I_{ref} equals I_d (discharging current for battery) or I_c (charging current for battery). As soon as the SOC reaches the limit value, the tertiary control-enabled signal is triggered and tertiary control starts to operate. However, based on Figure 6.12, the secondary control achieves voltage recovery by sourcing or sinking more current, which will cause the battery SOC to reach the SOC limit faster. Therefore, the secondary control will be disabled when tertiary control begins to operate. The tertiary controller can be represented as

$$V_c = \frac{k_{cp}(I_{ref} - I_b) + k_{ci}(I_{ref} - I_b)}{s} \tag{6.6}$$

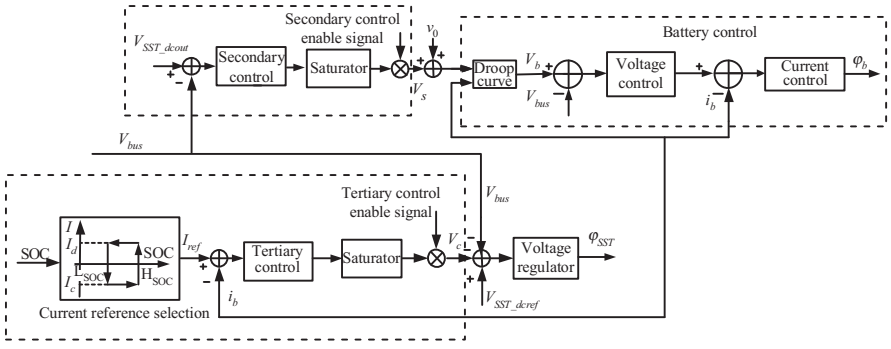

Figure 6.13 First tertiary control diagram of the DC microgrid system

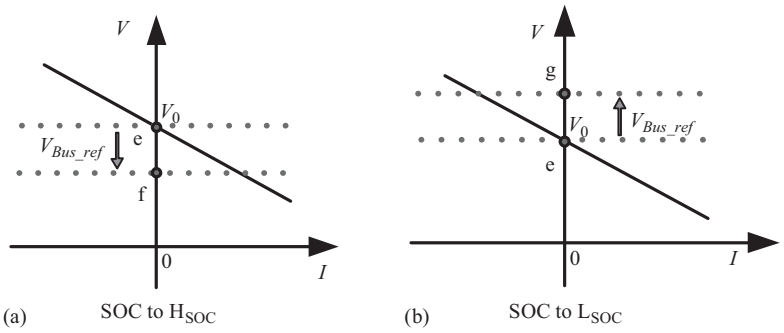

Figure 6.14 SST DC voltage shift in the tertiary control shown in Figure 6.13: (a) SOC to higher boundary and (b) SOC to lower boundary

where k_{cp} and k_{ci} are the tertiary control parameters. The bus voltage reference can be as shown in (6.7):

$$V_{Bus\_ref} = V_{SST\_dcref} - V_c \tag{6.7}$$

As shown in Figure 6.14(a), for example, if I_{ref} equals I_d, the bus voltage operation point will shift from point e to point f. Here, the bus voltage is less than the V_0 for battery droop curve. Thus, the battery will switch to discharging mode automatically. When SOC reaches L_{SOC}, the SST DC output voltage will be higher than V_0 (point e to point g) and the battery will be charged [see Figure 6.14(b)].

Shifting battery droop curve

As in the previous tertiary control scheme, the current reference is determined by the current reference selection block based on the SOC. If the SOC reaches the H_{SOC}, I_{ref} equals I_d. Or if the SOC reaches the L_{SOC}, I_{ref} equals I_c. In contrast to the aforementioned tertiary control scheme, the battery droop curve is changed instead of the SST DC bus voltage. Then the tertiary controller can be represented as following:

$$V_t = \frac{k_{tp}(I_{ref} - I_b) + k_{ti}(I_{ref} - I_b)}{s} \tag{6.8}$$

where K_{tp} and k_{ti} are the control parameters for the tertiary controller. Therefore, for battery droop control, (6.5) becomes

$$V_b = V_0 - R_b I_b + V_t \tag{6.9}$$

The secondary control will be disabled at the time which or before the tertiary control starts. The key point for this tertiary control scheme is to shift the droop curve as shown in Figure 6.15. When the battery SOC is low, the droop curve will shift down, and vice versa. Since the PV and load control do not contribute to regulate the DC bus voltage, their control is the same as shown in Figure 6.10. Due to the space limitations, only the battery module control is depicted in Figure 6.16.

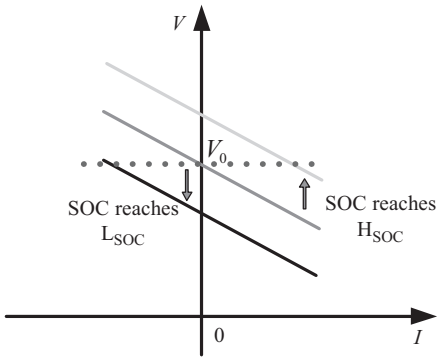

Figure 6.15 Droop curve shift with second tertiary control shown in Figure 6.13

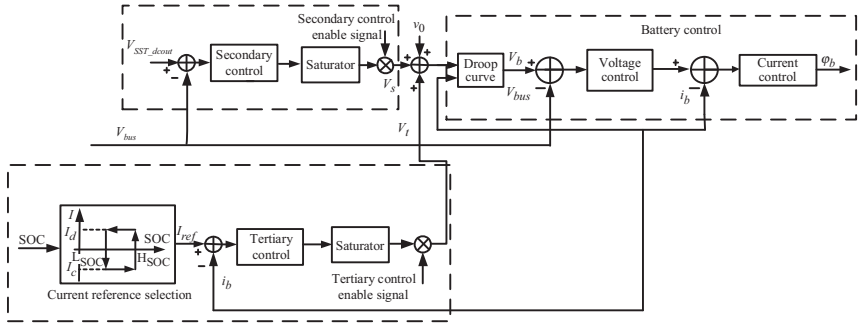

Figure 6.16 Second tertiary control diagram shown in Figure 6.13

6.4.2 Case study of a small-scale DC microgrid

To verify the primary control algorithm shown in Figure 6.10, an experiment is carried out on a lab test-bed. A 500-W battery module and a 200-W PV module are constructed to constitute the DC microgrid. The input voltage of the SST is 1.2 kV, the low voltage DC link is 380 V, and the low voltage AC link is 240-V AC. When the PV generation unit is operating with MPPT control, the maximum power is 100 W and the corresponding MPPT voltage is about 48 V. The nominal battery voltage is 48 V and the capacity is 20 A h.

6.4.2.1 Case I: Primary control of the SST-enabled DC microgrid system

To verify the primary control algorithm, an experiment is carried out in the test-bed. The DC microgrid operates in islanding mode and the result is depicted in Figure 6.17. Initially, only the battery supplies power to the load (2 kΩ). Then the PV connects to the system and supply the power to the load. Since the PV's output

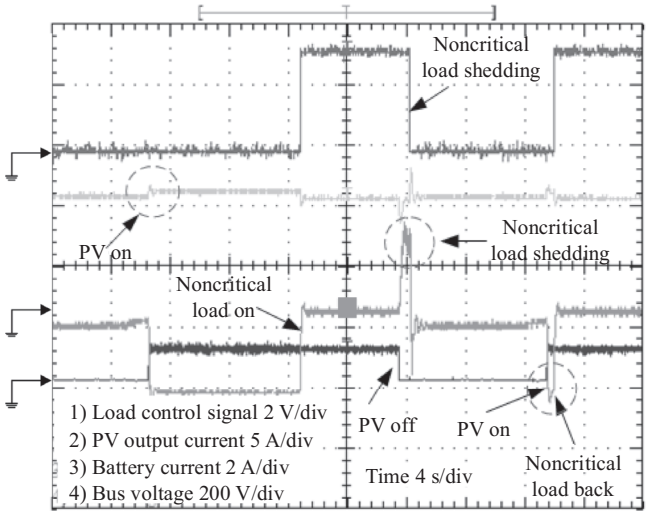

Figure 6.17 Waveforms from the primary control

power is larger than the load, the battery switches to the charging mode automatically and the bus voltage is higher than 380 V. When the noncritical load (1 kΩ) connects to the system, the bus voltage drops and the battery switches back to the discharging mode. Since the bus voltage exceeds the 370 V (value for load shedding), the noncritical load remains connected to the bus. After the PV disconnects from the system, the battery has to supply the power to the load alone and the bus voltage decreases. After 0.5 s when the bus voltage drops below 370 V, the noncritical load is shed from the system, and the bus voltage can recover. When the PV is connected back to the system the bus voltage increases. After 0.5 s when the bus voltage again exceeds 380 V (the value for noncritical load back), the noncritical load is reconnected to the system automatically.

6.4.2.2 Case II: Secondary control of the SST-enabled DC microgrid system

To verify the secondary control algorithm, experimental results are shown in Figure 6.18. The communication ports are not included in this chapter, so a software trigger is used to start the secondary control; the time step for secondary control is 1 ms.

Figure 6.18(a)–(c) shows the waveforms with the secondary controller. Figure 6.18(a) shows the SST waveforms, including the input voltage and current, high voltage DC of one AC/DC power stage, and low-voltage DC. In Figure 6.18(b), before the secondary control loop starts, the DC microgrid bus voltage is less than 380 V because the battery and the PV have been supplying the power to the load. As soon as the secondary control loop begins to operate, the microgrid bus voltage increases with the secondary control time step until it reaches 380 V. Then the DC

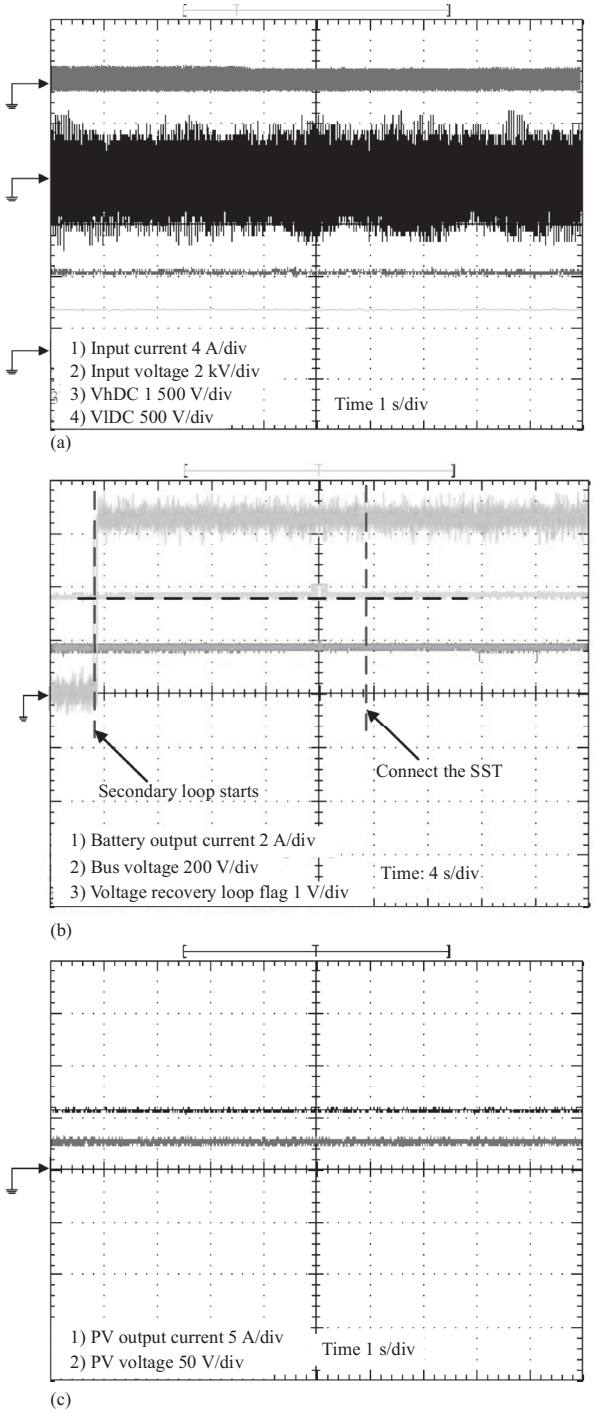

Figure 6.18 Waveforms with secondary control for the system in Figure 6.2: (a) SST waveforms, (b) battery current, DC microgrid bus voltage, and SST AC output, (c) PV waveform

microgrid connects to the SST, and a seamless transfer is achieved. Furthermore, the battery droop curve is lifted based on the secondary control loop as previously described. Therefore, when the system is in SST-enabled mode, the battery still outputs current to the load. For the PV module, there is no change in its output voltage and current because it always operates in the MPPT mode as shown in Figure 6.18(c).

6.4.2.3 Case III: First tertiary control

To verify the first tertiary control algorithm, experimental results are shown in Figure 6.19. SOC estimation is beyond the focus of the chapter, and therefore, it is not covered here. A software trigger is used to start the tertiary control, emulating the time when the battery SOC reaches its upper limit.

Figure 6.19(a) shows the SST waveforms, including the input voltage and current, high-voltage DC of one AC/DC power stage, and low-voltage DC. When the tertiary control starts, the SST output DC bus voltage increases because the V_c in (6.7) is less than zero. Figure 6.19(b) shows the SST AC-side voltage, DC microgrid bus voltage, and the battery current. It is noted that the secondary control is disabled before the tertiary control starts. Therefore, the battery module's output current is almost zero before the tertiary control starts. When the tertiary control starts, the DC bus voltage increases until the battery output current reaches its current reference (−2 A). Since the PV is still in the MPPT mode, its curve is same as the previous case, which is shown in Figure 6.19(c).

6.4.2.4 Case IV: Second tertiary control

To verify the second tertiary control algorithm, experimental results are shown in Figure 6.20. Similarly, a software trigger is used to start the tertiary control to emulate when the SOC reaches the L_{SOH}, and the time step for tertiary control is 0.1 s.

Figure 6.20(a) shows the SST waveforms, including the input voltage and current, high-voltage DC, and low-voltage DC. When the tertiary control starts, in contrast to the previous tertiary control, the SST output DC bus voltage remains constant at 380 V. Figure 6.20(b) shows the SST AC-side voltage, DC microgrid bus voltage, and the battery current. When the secondary control loop stops, the battery output current drops to zero because the V_0 equals 380 V (the SST DC output voltage) without the voltage recovery item (i.e., V_s is zero). After the battery's output current reaches zero, the tertiary control loop is triggered and begins to operate (the green line goes to 3.3 V). Then the battery starts to charge until the current reaches the I_c value (−2 A). As with the first tertiary control method, the PV is still in MPPT mode, and there is no change in its waveform whether the secondary control stops or tertiary control starts, as shown in Figure 6.20(c).

6.4.2.5 Comparison of the two tertiary control methods

The first tertiary control has the following disadvantages: (1) when the DC bus voltage changes, the load power changes; (2) the DC bus voltage range is limited

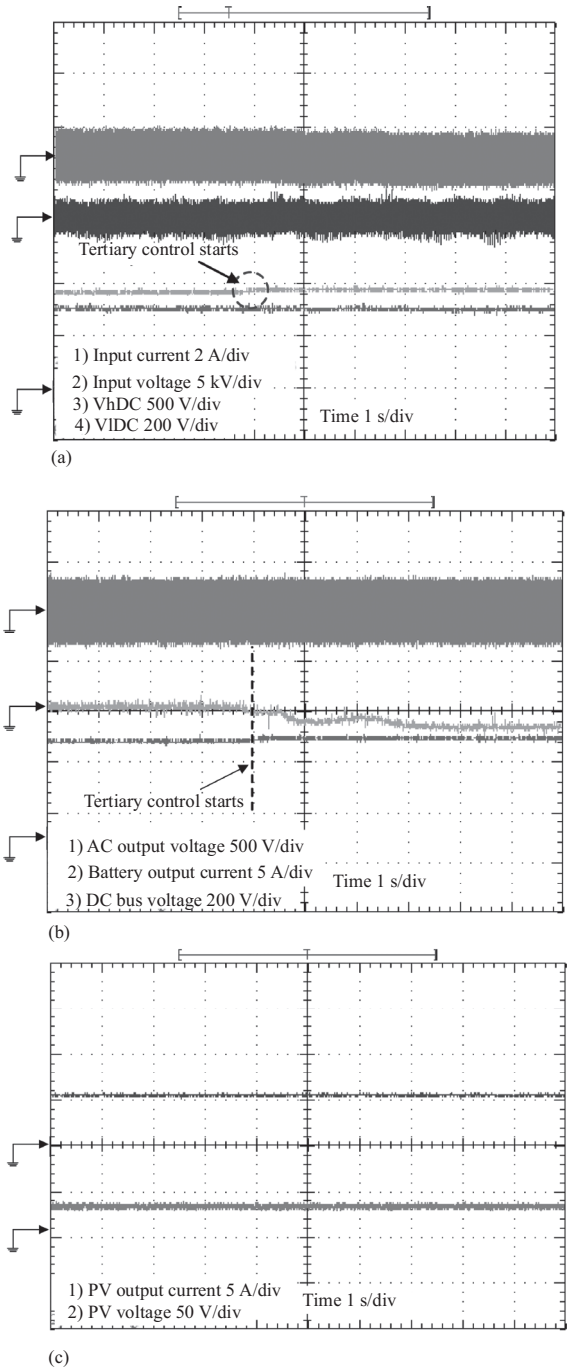

Figure 6.19 Waveforms with first tertiary control principal: (a) SST waveform, (b) battery current, DC microgrid bus voltage, and SST AC output, (c) PV current and voltage

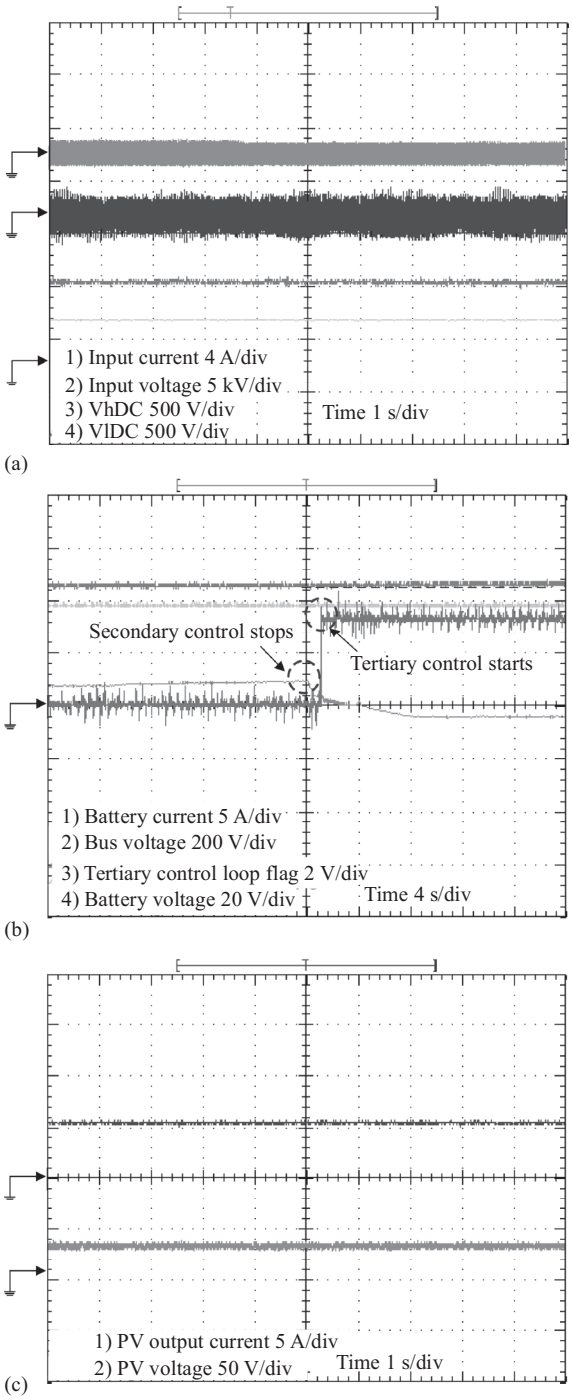

Figure 6.20 Waveforms with second tertiary control: (a) SST waveform, (b) battery current, DC microgrid bus voltage, and control flag, (c) PV waveform

by the SST output voltage range. When the charging and discharging current references are large, the SST output DC voltage might reach its limitation and then the battery's output current cannot match with the references. Compared to the first tertiary control method, the second tertiary control method does not have these two problems since it just changes the battery's droop curve. However, its disadvantage is that communication ports need to be involved because the control output commands need to be sent from the SST to the battery module, which will degrade the system reliability. For the first tertiary method, the communication is exclusive since the control method is only implemented on the SST side. Which method to select will depend on the designer and the system requirements.

6.4.3 Summary

A hierarchical power management strategy for the SST-based DC microgrid is proposed, which includes primary control, secondary control, and tertiary control. The DC microgrid not only can operate more reliably in islanding mode by primary control, but can also seamlessly transfer the DC microgrid from islanding mode to SST-enabled mode via secondary control. The battery SOC is involved in the tertiary control for battery management. Experimental results are presented to verify the proposed schemes.

6.5 Control of SST-enabled DC microgrid as a solid-state synchronous machine (SSSM)

6.5.1 Concept of the SSSM

The SST-enabled DC microgrid integrates DRER, distributed energy storage devices (DESD) and DC loads, and interfaces to the legacy grid by a phase locked loop (PLL). Traditionally, the SST is controlled as a current source and from the grid point of view, the SST-enabled DC microgrid lacks the rotational inertia of a traditional synchronous generator, which follows the grid frequency and the high-power intermittence of DRER, and load is instantaneously reflected at the point of common coupling. The concept of SSSM is proposed to overcome the frequency and voltage instability issues in a high DRER penetration system [5–7].

Figure 6.21 shows the overall architecture of an SST-enabled DC micro-grid when it is controlled as an SSSM. The detailed control diagram applied in single-phase inverter is shown in Figure 6.22. The SST interfaces the DC microgrid to legacy grid with frequency and voltage regulation capabilities. The microgrid acts as a voltage source which mimics the behavior of the synchronous machine to form the grid. It improves the aforementioned SST-enabled DC microgrid with (1) a larger inertia; (2) a simple and extendible model for large-scale power system analysis; (3) no use of PLL during normal operation; (4) seamless transition from grid-connection mode to islanding mode; (5) up/down reserve for frequency regulation with the support of energy storage (battery).

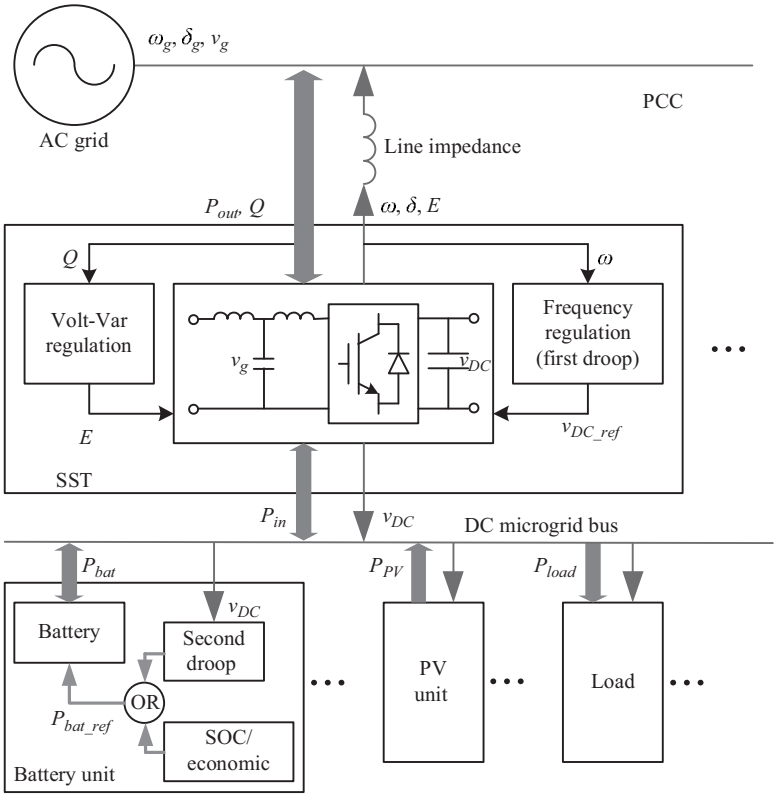

Figure 6.21 Overall architecture of the SST-enabled DC microgrid as an SSSM with the associated control strategy

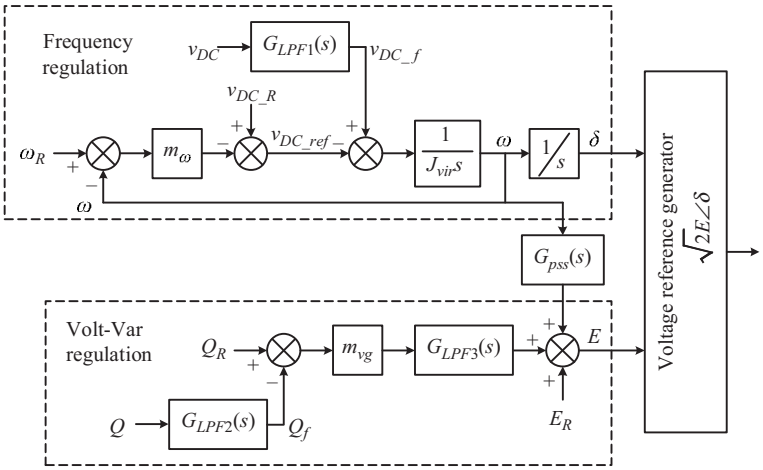

Figure 6.22 Detailed control strategy diagram of the SST controlled as SSSM

6.5.2 Frequency regulation

The traditional SM rotor's mechanical characteristic is called the swing equation and expressed as

$$J\frac{d\omega_r}{dt} + D(\omega_r - \omega_g) = T_m - T_e \tag{6.10}$$

where ω_r is the rotor angular frequency, ω_g is the grid frequency, J is the angular momentum inertia of the rotor, D is the damping coefficient generated by the damper windings, and T_m and T_e are the input mechanical torque and load electric torque, respectively. The dynamics of SM rotor is normally slow due to the large J. In the SST, the dynamic equation of the DC voltage with a DC capacitor C_{DC} can be derived as

$$C_{DC}v_{DC}\frac{dv_{DC}}{dt} = i_{in}v_{DC} - i_{out}v_{DC} = P_{in} - P_{out} \tag{6.11}$$

Equation (6.11) is similar with (6.10), where $C_{DC}v_{DC}$, V_{DC}, P_{in}, and P_{out} are, respectively, corresponding to J, ω_r, T_m, T_e. Assuming that SST is lossless, P_{out} is also the output active power into the AC grid. Equation (6.11) shows that the DC capacitor has similar dynamics with the SM rotor and can be used for the inertia emulation. But in order to get the same inertia as the SM rotor, the DC capacitor will be very large.

The equation of the frequency regulation in Figure 6.23 is derived as

$$J_{vir}\frac{d\omega}{dt} + m_\omega(\omega - \omega_R) = G_{LPF1}(s)v_{DC} - v_{DC\_R} \tag{6.12}$$

Equation (6.12) is also similar with (6.10), where the virtual inertia parameter J_{vir} and damping coefficient m_ω are, respectively, corresponding to J and D. So this regulation can also emulate the SM rotor's characteristic without physical component. The difference is that the torque is replaced by V_{DC}, and the dynamic equation (6.11) is then inserted in the swing equation. G_{LPF1} is a first-order low-pass filter used to suppress the low-order harmonics for V_{DC}.

The virtual rotor model of the SSSM concept-based SST is developed based on (6.11) and (6.12), as shown in Figure 6.23 in s-domain. When P_{in} or P_{out} varies, the difference between them will change V_{DC} based on C_{DC}, and then ω based on J_{vir}. This will change δ and then P_{out} according to the power–angle relationship. Finally,

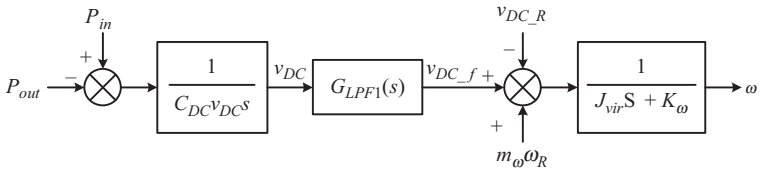

Figure 6.23 Block diagram of the SST's virtual rotor model

a new balanced working point for P_{in}, P_{out}, and δ is reached, while ω synchronizes with ω_g again. The microgrid's total inertia is determined by C_{DC}, V_{DC}, ω_{c1}, and J_{vir}. When C_{DC} is designed normally, J_{vir} will be an extra control parameter to adjust the inertia to meet the stability requirement in the power system.

According to the analysis above, any power from the DC microgrid can be transmitted to the AC grid through the SST at a given AC frequency. The dynamics of AC output active power is slowed down and completely decoupled from the intermittent, variable DRERs and loads at the DC microgrid. So this microgrid's model is simple and promising for studying the scalability and stability of the paralleled systems. Due to its swing characteristic, the microgrid is able to respond to the short-term requirements of the grid frequency regulation.

6.5.3 Power up/down reserve support

Different from the traditional SST control that synchronizes with power grid with no frequency response, the SSSM-based SST will supply the power system with up/down power reserve with its emulated angular speed ω and support of energy storage units such as supercapacitor or battery. Dual droop control, as shown in Figure 6.24 is proposed to coordinate the SST with DESD and implement the up/down reserve for primary frequency regulation, similar to the governor control in synchronous machine.

1. *First droop in SST:* Since the energy storage units in the DC microgrid only react to V_{DC}, ω in the SST must be linked to V_{DC} through the active power. The traditional droop controls for active power in AC and DC system, respectively, are

$$\omega - \omega_R = -k_\omega (P - P_{rate}) \tag{6.13}$$

$$v_{DC} - v_{DC\_R} = -k_{vDC} (P - P_{rate}) \tag{6.14}$$

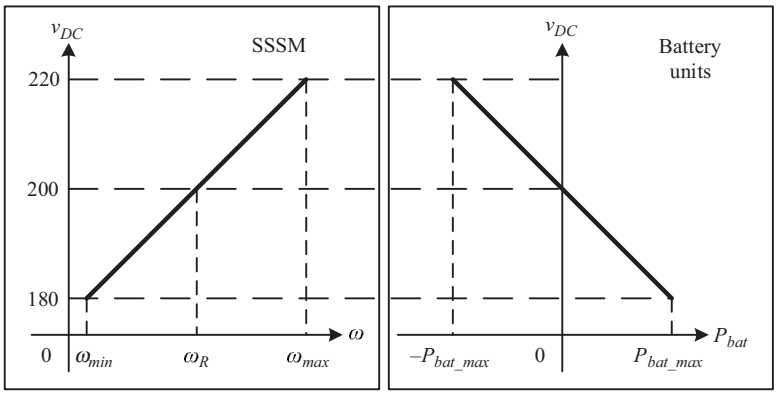

Figure 6.24 Detailed diagram of dual droop control for SSSM and battery units' coordination

where P_{rate} is the converters' rated power, and k_ω and k_{vDC} are the droop slopes for AC and DC systems. Combining (6.13) and (6.14), the first droop in the SST can be rewritten as

$$v_{DC} - v_{DC\_R} = \frac{k_{vDC}}{k_\omega}(\omega - \omega_R) = m_\omega(\omega - \omega_R) \tag{6.15}$$

In (6.15), m_ω is determined by the allowable ranges of ω and V_{DC}. Typically, $1/k_\omega$ is proportional to the SST's rated power. The DC voltage ranges are designed to be the same for different SSTs, then $1/k_{vDC}$ is also proportional to their rated power, and the resulting m_ω will be the same for different SSTs. For the frequency regulation control in Figure 6.23, this droop control is naturally integrated in it, and m_ω is also the coefficient for the part of the damping.

2. *Second droop in energy storage units:* The second droop in the energy storage units is a traditional V–P droop, and m_{vDC} is its droop slope. According to the first droop in the SST, P_{bat} should be controlled based on V_{DC}. This control is shown in the right column in Figure 6.24. The hierarchical power management discussed in Section 6.4 for battery is still applicable as an offset power reference.
3. *Coordination of dual droop:* Figure 6.25 shows the coordination diagram of the dual droop control. V_{DC} is controlled according to ω through the first droop. This voltage is a command, which indicates the energy storage units how much power SST requires corresponding to the second droop curve. Then energy storage units will output the corresponding power through the second droop and inject it into the AC grid via the SST. This is similar to the traditional active power control in the SM, and finally, the SST with the DC microgrid will have the ω–P droop characteristic.

The dual droop control is distributed and autonomous without communication. In steady state, the SSTs connected to the same AC grid will synchronize with it, share and balance the power via the AC frequency. So the SST can provide up/down reserve to the grid when ω_g varies in a desirable region, with the support from energy storages. The power in the DC microgrid is also shared and balanced based on the second droop among paralleled energy storage units. So the power management of the AC grid and DC microgrid are achieved simultaneously either in

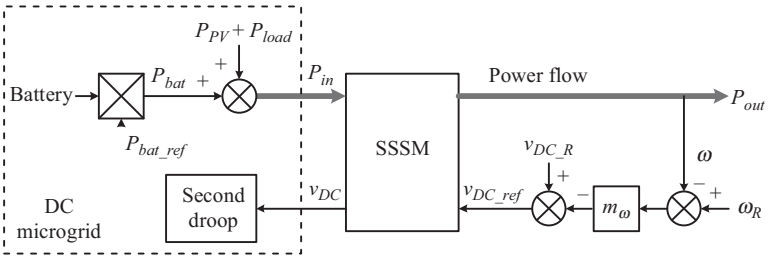

Figure 6.25 Coordination diagram of a dual droop control

grid-connection or islanding modes. During the dynamics, the dual droop control will also support the demanded inertia at a given ω_g. It is achieved by commanding energy storages to provide temporary energy to the SST through V_{DC}, when ω and V_{DC} vary due to the disturbances from the AC grid or DC microgrid.

6.5.4 Voltage regulation

In Figure 6.22, a simple *Volt-Var* droop control (shown in Figure 6.26) is adopted to mimic the excitation system of SMs, where m_{vg} is its droop slope. In SMs, the exciter is usually a proportional controller, and the field circuit flux is produced based on it after a long-time delay. To emulate this, a first-order LPF can be adopted, shown as $G_{LPF3}(s)$ in Figure 6.22.

6.5.5 Case study

To verify the primary control algorithm, a low-power experiment is carried out in the lab test-bed. A 500-W battery module, a 500-W PV module, and up to 500-W DC load are constructed to constitute the DC microgrid. The grid voltage of the 1,200-W SST is 120 V, and the DC link voltage is 200 V. When the PV generation unit is operating with MPPT control, the maximum power is 500 W, and the corresponding MPPT voltage is about 28 V. The nominal battery voltage is 12 V and the capacity is 20 A h. $m_\omega = 31.83$ is chosen so that V_{DC} works from 180 to 220 V, when ω works from 59.9 to 60.1 Hz; $m_{vg} = 0.005$ is chosen so that E will work from 114 to 126 V when the virtual synchronous machine based interface (VSMBI) provides 100% to −100% reactive power to the grid. The constant $m_{vDC} = 25$ is chosen, so that battery will operate from 180 to 220 V with 500-W discharge to 500-W charge power.

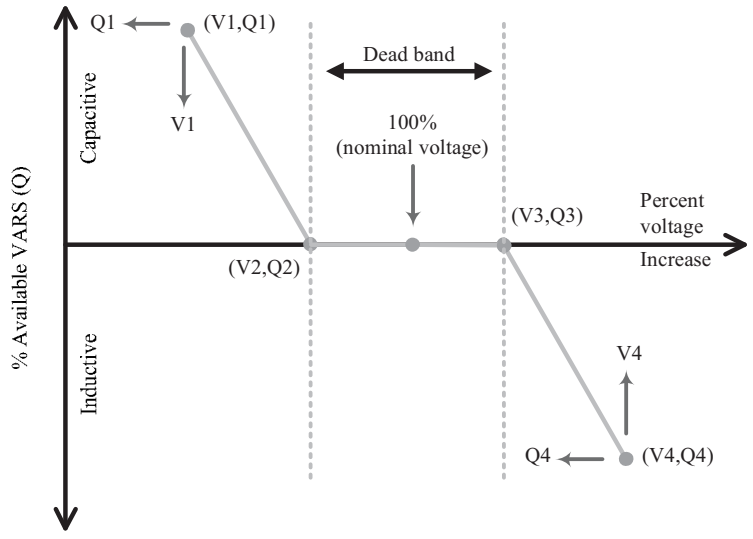

Figure 6.26 Volt-Var droop control of SSSM applied in Figure 6.22

6.5.5.1 Case I: Load change

In this case, an 80-Ω resistance load is disconnected first, and then reconnected. Figure 6.27 shows the results when J_{vir} is separately set at 1.06 and 4.24. The system will take about 1.7 and 2 s to reach new operating points in Figure 6.27(a) and (b), compared with 2 and 2.1 s in Figure 6.27(c) and (d). These results verify the effectiveness and functions of the SST with the DC microgrid as SSSM in generator mode.

6.5.5.2 Case II: Source change

In this case, PV output current changes from 2.5 to 0 A first, and then changes back. Figure 6.28 shows the results when J_{vir} is set at 1.06 and 4.24. The system takes about 1.6 and 1.2 s to reach new stable working points in Figure 6.28(a) and (b), compared with 2.6 and 2 s in Figure 6.28(c) and (d). The system's functions in motor mode are verified.

6.5.5.3 Case III: Power up/down reserve

Figure 6.29 shows the results for 200 s when everything is in default settings. ω varies with the time, because ω_g is varying and ω is synchronizing with it. The frequency variation is normal in utility grid due to the customers' load change, and

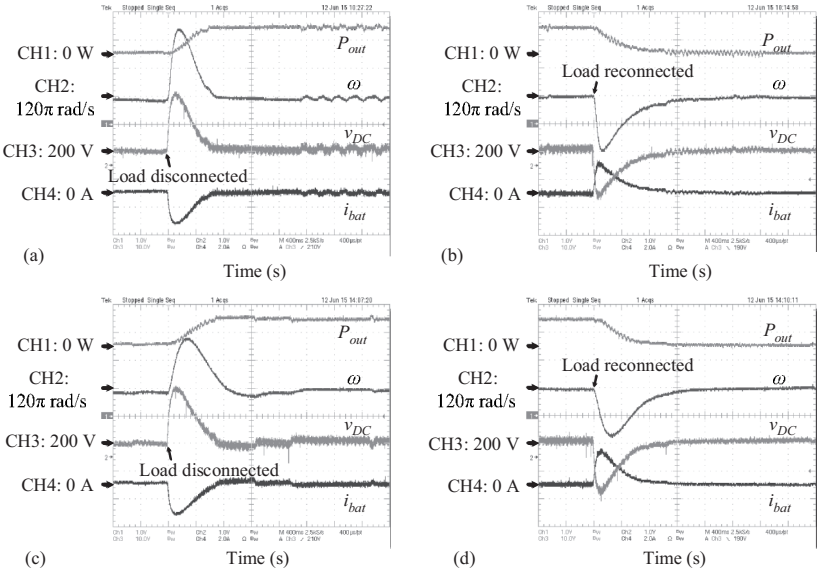

Figure 6.27 Experimental results of Case I: (a) $J_{vir} = 1.06$, 80-Ω load changes to no load; (b) $J_{vir} = 1.06$, no load changes to 80-Ω load; (c) $J_{vir} = 4.24$, 80-Ω load changes to no load; (d) $J_{vir} = 4.24$, no load changes to 80-Ω load. CH1: P_{out} (500 W/div); CH2: ω (0.08 π rad/s/div); CH3: v_{DC} (10 V/div); CH4: i_{bat} (2 A/div); X-axis: time t (400 ms/div)

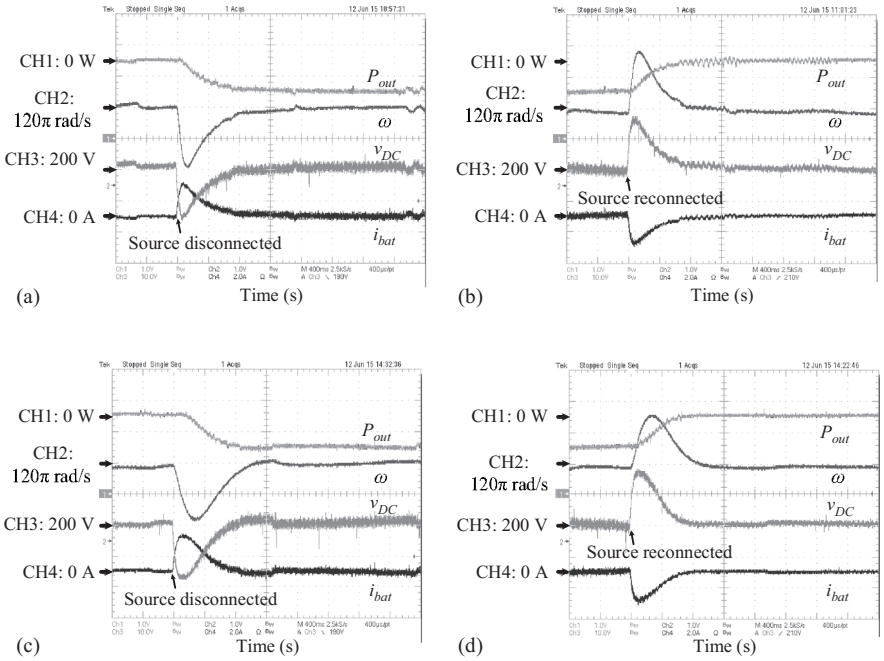

Figure 6.28 Experimental results of Case II: (a) $J_{vir} = 1.06$, 2.5-A source changes to 0 A; (b) $J_{vir} = 1.06$, 0-A source changes to 2.5 A; (c) $J_{vir} = 4.24$, 2.5-A source changes to 0-A; (d) $J_{vir} = 4.24$, 0-A source changes to 2.5 A. CH1: P_{out} (500 W/div); CH2: ω (0.08 π rad/s /div); CH3: v_{DC} (10 V/div); CH4: i_{bat} (2 A/div); X-axis: time t (400 ms/div)

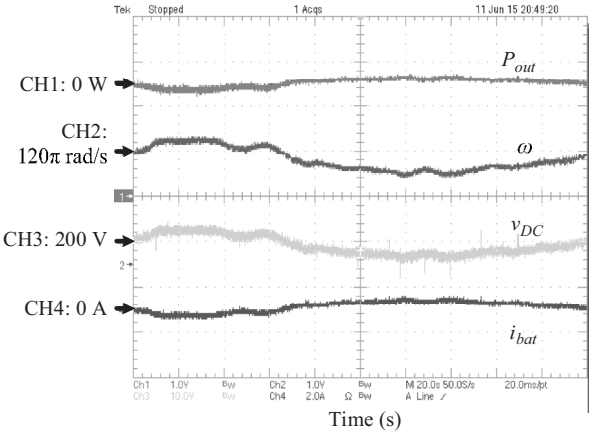

Figure 6.29 Experimental results of Case III: CH1: P_{out} (500 W/div); CH2: ω (0.08 π rad/s /div); CH3: v_{DC} (10 V/div); CH4: i_{bat} (2 A/div); X-axis: time t (20 s/div)

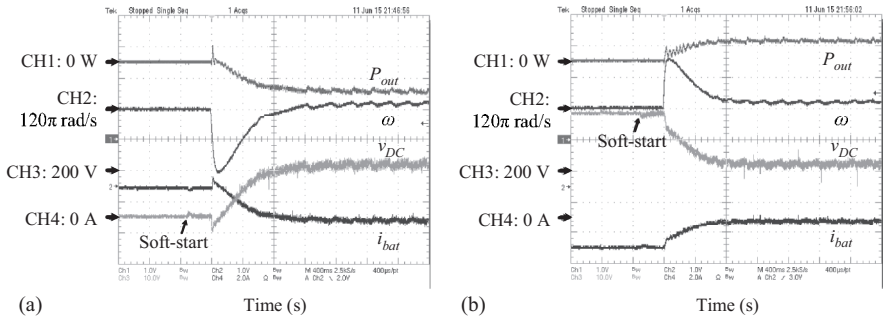

Figure 6.30 Experimental results of Case IV: (a) reconnecting with battery unit and load and (b) reconnecting with battery unit and current source. CH1: P_{out} (500 W/div); CH2: ω (0.08 π rad/s /div); CH3: V_{DC} (10 V/div); CH4: i_{bat} (2 A/div); X-axis: time t (400 ms/div)

it is the reason why sometimes ω and V_{DC} do not work at the rated values in Figures 6.27 and 6.28. Since the proposed system can synchronize its own frequency with ω_g with a high degree of accuracy, it can also work as a phasor measurement unit in the power systems. In Figure 6.29, V_{DC} and i_{bat} vary and follow ω according to the dual droop control. This verifies the effectiveness and functions of the dual droop control in the proposed concept, supplying the power system with up/down reserve when the frequency deviates from the rated 60 Hz.

6.5.5.4 Case IV: Islanding and reconnection

In this case, at first the AC grid is disconnected, SST stops working and the DC microgrid keeps working. Figure 6.30(a) shows the transition for the system reconnecting and synchronizing with the AC grid when only battery unit and 400-W load are present, and Figure 6.30(b) shows the transition when only battery unit and 2-A DC source are present. Initially, i_{bat} is about 1.95 and −2.1 A, respectively, and V_{DC} is about 185.5 and 218.5 V; the system takes about 1.4 and 1.3 s to reconnect, as shown in Figure 6.30. The achievement of power management in DC microgrid when SST is not working and the proposed concept's synchronization capability are verified.

6.5.6 Summary

An SSSM concept is proposed to integrate the DC microgrid into legacy AC grid through an SST. The benefits are (1) integrates the DERs, loads, and energy storages in the DC microgrid into SSSM; (2) achieves power management for the AC grid and DC microgrid, and enable the DERs and loads to output any power at a given AC frequency; (3) introduces inertia, provides up-reserve and down-reserve for the grid with support from practical energy storages, and decouples the AC output from the fast responding DERs and loads. Experimental results verify the effectiveness and the benefits of the presented method.

6.6 Conclusion

The SST-enabled DC microgrid concept is introduced in this chapter. Compared to the traditional microgrids, the presented system enables a compact and integrated interface for the DC and AC grids. Centralized power management strategy, hierarchical power management strategy, and SSSM concept are proposed to control the operation of the presented system. Simulation and experimental results are given to demonstrate the feasibility of the proposed system.

References

[1] X. She, A. Q. Huang, and R. Burgos, "Review of Solid-State Transformer Technologies and Their Application in Power Distribution Systems," *IEEE J. Emerg. Sel. Topics Power Electron*., vol. 1, no. 3, pp. 186–198, September 2013.

[2] X. She, A. Q. Huang, S. Lukic, and M. Baran, "On Integration of Solid-State Transformer with Zonal DC Microgrid," *IEEE Trans*. *Smart Grid*, vol. 26, no. 12, pp. 3778–3789, June 2012.

[3] J. M. Guerrero, J. C. Vasquez, J. Matas, L. Vicuna, and M. Castilla, "Hierarchical Control of Droop-Controlled ac and dc Microgrids – A General Approach Toward Standardization," *IEEE Trans. Ind. Electron.*, vol. 58, no. 1, pp. 158–172, May 2011.

[4] X. Yu, X. She, X. Ni, and A. Q. Huang, "System Integration and Hierarchical Power Management Strategy for a Solid-State Transformer Interfaced Microgrid System," *IEEE Trans. Power Electron.*, vol. 29, no. 8, pp. 4414–4425, August 2014.

[5] M. Ashabani, and Y. A.-R. I. Mohamed, "Novel Comprehensive Control Framework for Incorporating VSCs to Smart Power Grids Using Bidirectional Synchronous-VSC," *IEEE Trans*. *Power System*, vol. 29, no. 2, pp. 805–814, March 2014.

[6] Q. Zhong, and G. Weiss, "Synchronverters: Inverters that Mimic Synchronous Generators," *IEEE Trans. Ind. Electron.*, vol. 58, no. 4, pp. 1259–1267, April 2011.

[7] D. Chen, Y. Xu, and A. Q. Huang, "Integration of DC Microgrids as Virtual Synchronous Machines into the AC Grid," *IEEE Trans. Ind. Electron.*, vol. 64, no. 9, 7455–7466, September 2017.